VALIDATION OF AN OPERATIONAL LIGHTNING DETECTION SYSTEM

I. Holleman [1], H. Beekhuis [1], S. Noteboom [1,2], L. Evers [1], H. Haak [1],
H. Falcke [3,4], and L. Bähren [3,4]

(1) Royal Netherlands Meteorological Institute (KNMI)
De Bilt, Netherlands
(2) Wageningen University and Research center (WUR)
Wageningen, Netherlands
(3) Netherlands Foundation for Research in Astronomy (ASTRON)
Dwingeloo, Netherlands
(4) Department of Astronomy, Radboud University,
Nijmegen, Netherlands

1. GENERAL INTRODUCTION

At the previous International Lightning Detection Conference (ILDC 2004) in Helsinki, Beekhuis and Holleman (2004) presented the upgrade and evaluation of the KNMI lightning detection system. Since 1995 KNMI operates a SAFIR (Surveillance et Alerte Foudre par Interférométrie Radioélectrique) Lightning Detection System for monitoring (severe) convection and for feeding a climatological database. In 2003 the lightning detection stations and the central processor (application and hardware) have been replaced.

During this replacement the performance of the new lightning detection system has been compared with that of the old system. It was found that the total number of observed discharges, i.e., Cloud-to-Cloud (CC) and Cloud-to-Ground (CG) discharges, agrees rather well. However, the fraction of CG discharges with respect to the total number of discharges was seen to strongly depend on the configuration of the central processing application of the new SAFIR system. Without any reference observations of lightning activity and characteristics, it is thus not clear what the proper configuration of the lightning detection system should be.

Here we present three novel possibilities for objective validation of the lightning data of the SAFIR system. Validation against other operational lightning detection systems or manual observations of lightning is not discussed in this paper. The localization accuracy, detection probability, and false alarm ratio of the observed discharges are subject to the validation. The application of the following remote sensing systems for validation of the observed lightning discharges will be discussed:

1.1 Weather radar

KNMI operates two C-band Doppler weather radars that observe three-dimensional distribution of the reflectivity from precipitation every 5 minutes. The observed lightning discharges can be overlaid with the radar precipitation patterns and thus these discharges can be validated.

1.2 Infrasound

The Seismology division of KNMI operates a network of infrasound sensors. Both the direction and intensity of infrasound are measured with an array of micro-barometers in the range of 500 seconds to 20 Hz with amplitudes of less than 0.01 Pa. Thunder from lightning discharges can be detected and localized with the infrasound sensors.

1.3 LOFAR

ASTRON is building a new low-frequency digital radio telescope array with all-sky viewing and transient detection capability (LOFAR). In the first and fully funded phase LOFAR consists of an extensive network of approximately 7700 dipole antennas arranged in clusters that are spread out over an area of ultimately 160 km in diameter. The LOFAR sensors have a low band (10 – 80 MHz) and a high-band (120 – 240 MHz) element which record the power, phase, and direction of the received radiation. Prototypes show that LOFAR detects lightning discharges with a high temporal and spatial resolution and is able to measure their broad-band spectrum.
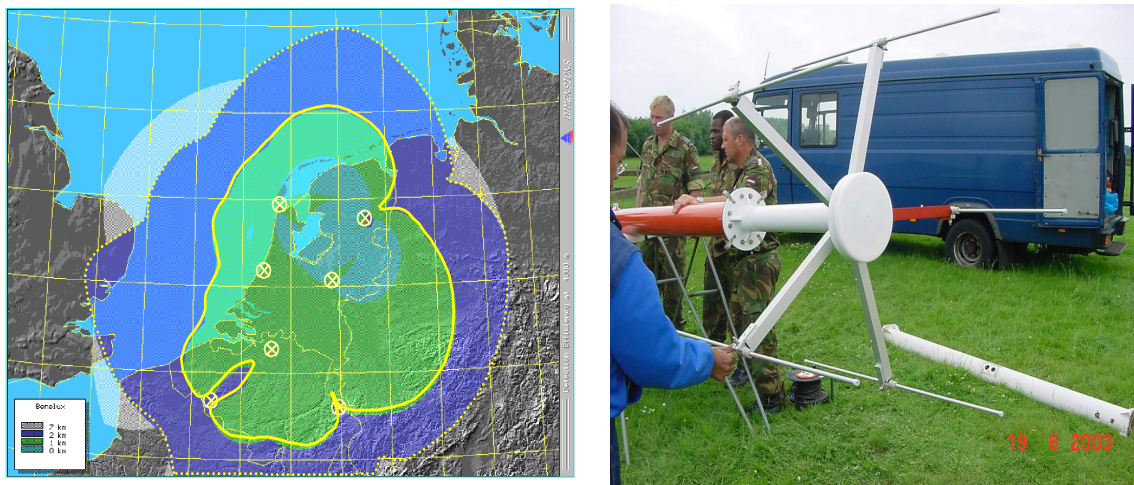
Figure 2.1: The left map shows the 7 lightning detection stations (4 in Netherlands and 3 in Belgium). The contours indicate the calculated localization accuracy. The right image shows the top of a detection tower with the VHF antenna array and LF sensor.

1.4 Outline

In this paper the preliminary results of the validation of lightning data from the KNMI-SAFIR system of with weather radar products, data from infrasound arrays, and retrievals from the LOFAR Initial Test-Station (ITS) are presented. In the next section the KNMI-SAFIR system is introduced and some details on the network are given. The use of the KNMI weather radar network for validation of the observed lightning discharges is discussed in section 3. Thunder signatures in data from an infrasound array are evaluated in section 4. In section 5 a first comparison of data from LOFAR ITS and the KNMI-SAFIR system is presented. It is concluded that these three remote sensing systems can provide a wealth of information on different aspects of lightning and thunder. This information may help to improve the performance of lightning detection systems and to increase our understanding of the complex processes inside a thunderstorm.

2. KNMI LIGHTNING DETECTION SYSTEM

KNMI operates a SAFIR (Surveillance et Alerte Foudre par Interférométrie Radioélectrique) Lightning Detection System for monitoring (severe) convection and for feeding a climatological database. The lightning detection system consists of four detection stations (SAFIR 3000 V3) located in the Netherlands and a central processing unit located at KNMI in De Bilt. In addition to the four Dutch stations raw data from three Belgium stations operated by RMI are processed in real time as well. A map with the locations of the seven detection stations and the calculated localization accuracy is shown in Figure 2.1 (left). Each lightning detection station consists of three basic components: a VHF antenna array (110 – 118 MHz), a LF sensor (300 Hz – 3 MHz), and a GPS receiver. An image of a SAFIR detection station is displayed in Figure 2.1 (right). The VHF antenna array consists of five dipole antennas mounted on a circle and is used for the azimuth determination of discharges based on interferometry. The capacitive LF antenna is used for lightning discrimination, i.e., Cloud-Ground (CG) or Cloud-Cloud (CC) discharge, and for Time-Of-Arrival (TOA) localization of discharges. The GPS receiver provides accurate time stamps for the observed discharges. The central processing application runs on a Windows 2000 cluster with redundant processors, hard disks, power supplies, etc.

The so-called SAFIR Control Module (SCM) acquires and processes data from the seven lightning detection stations. The SCM offers the possibility to apply two distinctly different algorithms to localize and discriminate the observed lightning discharges:

Direction finding (DF). In this mode, the discharge azimuths at the detection stations (determined using VHF interferometry) are used in a triangulation
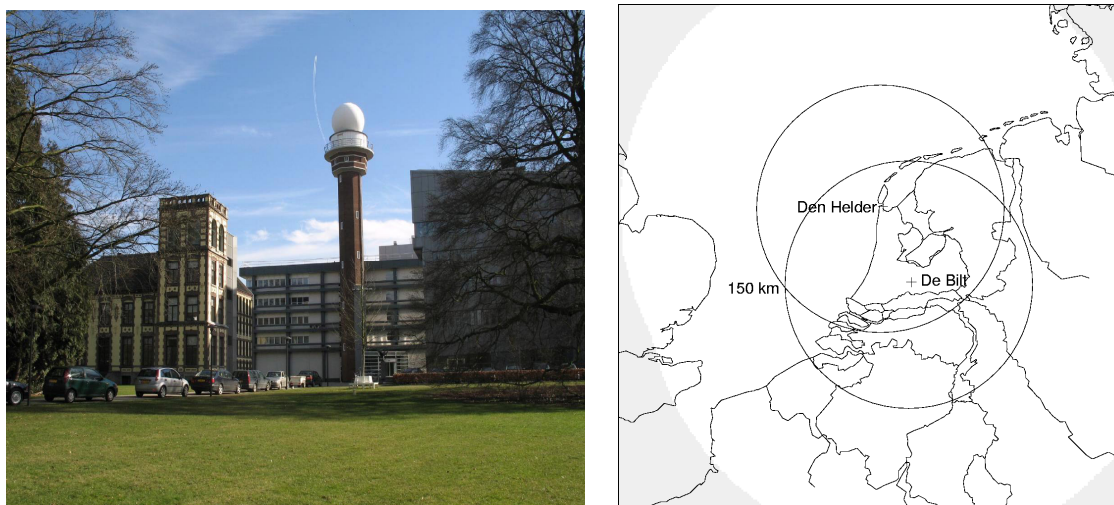
Figure 3.1: Picture of radar tower in De Bilt (left) and a map of the Netherlands with the locations of the two weather radars (right).

algorithm to localize the discharges. The observed shape of the LF pulse is used to discriminate between CC and CG discharges. A discharge is only classified as a CG when the observed rise time and decay time of the LF signal is within certain limits at a predefined number of detection stations (typically 3 or 4).

Time-Of-Arrival (TOA). In this mode, the VHF interferometry is only used to localize CC discharges and the TOA localization of the CG discharges is based on the time stamps of the signal peaks from the LF sensors. Given the time difference of a discharge observed at two stations, a hyperbola representing the possible locations of the discharge can be constructed. The intersection of hyperbolas obtained from different pairs of stations pinpoints the location of the discharge. It can be shown that at least four detection stations are required for an unambiguous localization. A discharge is only classified as a CG when it can be localized using the TOA technique which implies that it is observed by at least four detection stations.

As part of the upgrade of the lightning detection system, Beekhuis and Holleman (2004) have compared DF and TOA localizations and they concluded that the latter provides more accurate results.

At the central processor the lightning localization and discrimination data are converted into the HDF5 format (hdf.ncsa.uiuc.edu/HDF5) before distribution to the (real-time) users. The HDF5 data model used by KNMI is described in Roozekrans and Holleman (2003). This data model incorporates both an image and an indexed array with the localized discharges. A tool to list the HDF5 lightning data in a "one-event-per-line" layout on screen is available. The localization data are accumulated over 1 and 5 minutes for real-time use by duty forecasters and over 24-hours for off-line use by e.g. climatologists. More details on the technical layout of the KNMI lightning detection system can be found in Beekhuis and Holleman (2004).

3. WEATHER RADAR

A weather radar employs scattering of radio-frequency waves (5.6 GHz/5 cm for C-band) to measure precipitation and other particles in the atmosphere (See Doviak and Zrnić (1993) for more details). The intensity of the atmospheric echoes is converted to the so-called radar reflectivity Z using the equations for Rayleigh scattering. The Rayleigh equations are valid when the wavelength of the radar is much larger than the diameter of the scatterers

Table 3.1: Reflectivity versus Rain Rate

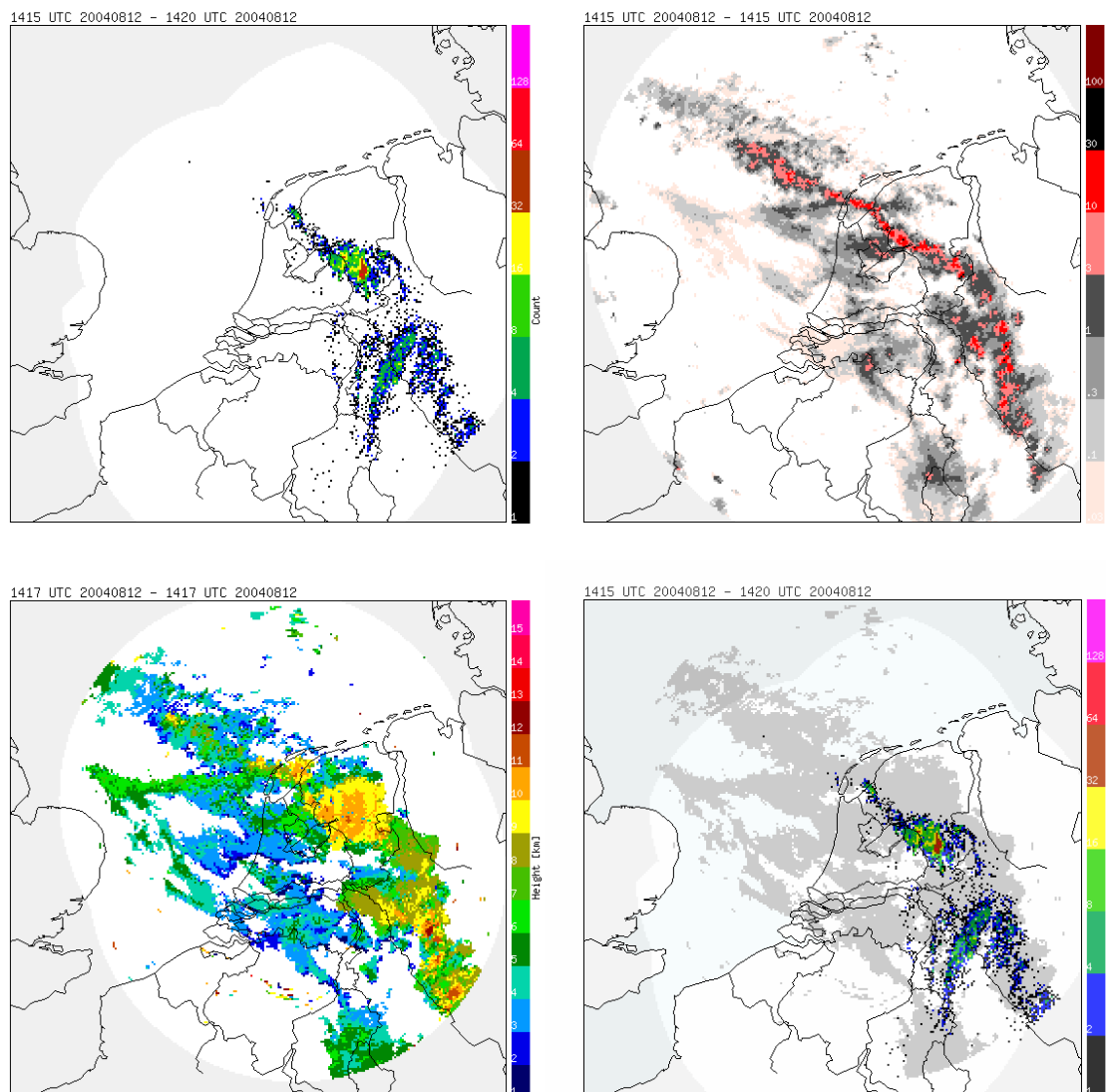| Z [dBZ]	7	15	23	31	39	47	55
R [mm/h]	0.1	0.3	1.0	3.0	10	30	100

Figure 3.2: Comparison of observed lightning discharges (upper left) and radar reflectivity at low altitude (upper right), and radar echotops (lower left) for 12 August 2004 at 1415 UTC. The lower right image shows the lightning discharges overlaid on the echotop contours.

(maximum 6 mm for rain). In that case, the radar reflectivity depends strongly (sixth power) on the diameter of the rain droplets. In Table 3.1 a few radar reflectivity values and corresponding rain rates are listed. The radar reflectivity is a good measure for the strength of the convection (updrafts) and the amount of moisture in the atmosphere. Strong updrafts of moist air are the main drive behind lightning activity, and therefore a strong correlation between radar reflectivity and the number of lightning discharges is expected. In other words, a lightning discharge observed in a clear-sky situation is suspicious.

KNMI operates two identical C-band Doppler weather radars from Gematronik GmbH. One radar is located in De Bilt (52.10N,5.18E) and the other one in Den Helder (52.96N,4.79E). The locations of the two radars are shown on the map in Figure 3.1. The circles indicate a range of 150 km from the radar sites which is roughly the maximum range for quantitative use of the data. The received signal is digested by a RVP6 radar processor (Sigmet Inc, www.sigmet.com) and the generation of radar products is done with the Rainbow package (www.gematronik.com).
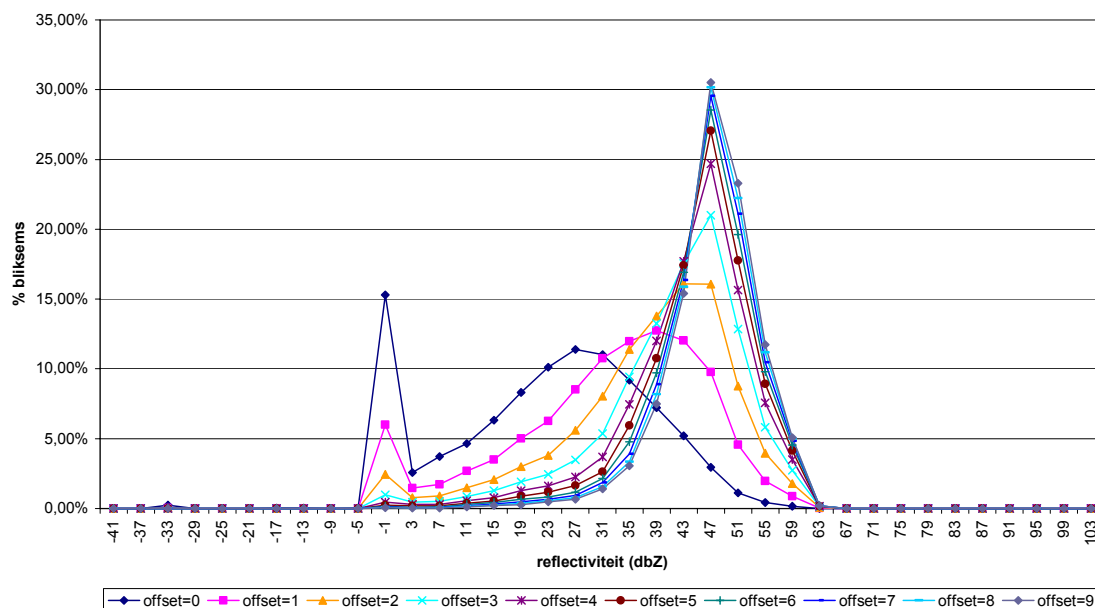
Figure 3.3: Histograms of the relative number lightning discharges per maximum radar reflectivity class (4 dBZ bins) for August 2004. The offset represents the "search radius" in units of image pixels (2.4 km).

3.1 Operational products

The operational reflectivity scans currently consist of a four-elevation scan (0.3 – 3 deg) every five minutes and a 14-elevation scan (0.3 – 12 deg) every 15 minutes. In addition, a five-elevation Doppler scan (2 – 25 deg) is performed every 15 minutes. The following products are produced operationally from the weather radar scans:

Reflectivity composites at low altitude (800 meter above msl). This main radar product showing the precipitation patterns is generated from the four-elevation scan.

Accumulated precipitation over 3 hour and 24 hour periods. The accumulations are based on the reflectivity composited and are adjusted with rain gauge observations.

Echotop height composites. This product showing the maximum height of the radar echoes is generated from the 14-elevation scan.

Hail warning product. Large hail is detected using the height difference between the 45 dBZ echotops and the freezing level from a Numerical Weather Prediction model (Holleman 2001).

Weather radar wind profiles extracted from the Doppler scans. A study focused on the optimization and verification of these wind profiles has been performed at KNMI (Holleman 2005).

The reflectivity composites and echotop maps will be used for validation of the lightning discharges observed with the SAFIR system. All weather radar products are available in the same KNMI HDF5 format as the lightning data (Roozekrans and Holleman 2003).

3.2 Comparison of lightning and radar imagery

The images with the observed lightning discharges and the radar reflectivity composites can easily be compared because the geographical projection and data format are identical. In Figure 3.2 the observed lightning discharges (upper left) and two different radar products are shown for a severe thunderstorm case on 12 August 2004. Between 1415 and 1420 UTC more than 600 discharges were observed over The Netherlands by the SAFIR system. On this afternoon an active squall line passed from south to north over The Netherlands. The radar reflectivity image of Figure 3.2 (upper right) clearly shows the intense squall line with a length of several hundreds of kilometers and a width of only 20 km. Comparing the two images a strong correlation between lightning discharges and the reflectivity pattern is
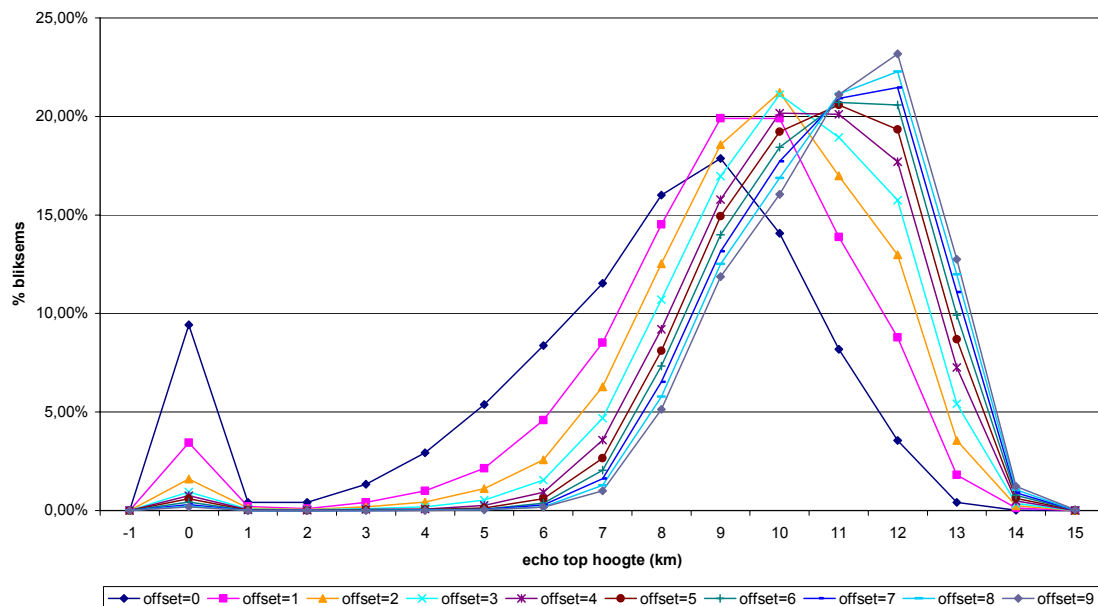
Figure 3.4: Histograms of relative number lightning discharges per maximum radar echotop height class (1 km bins) for August 2004. The offset represents the "search radius" in units of image pixels (2.4 km).

evident. The majority of the discharges coincides with the squall line in the reflectivity image. However, a large fraction of the discharges in the south-east quadrant of the image does not correspond very well with the low-altitude reflectivity pattern. These discharges probably originate from higher altitudes. The lower-left and lower-right images of Figure 3.2 show the corresponding radar echotop product and an overlay of the observed lightning discharges with the echotop contours, respectively. The spatial overlap is rather good and only a few discharges in the south-east quadrant are still not validated by the radar data.

3.3 Validation against the reflectivity composite

A quantitative comparison of the lightning and radar images has been performed for data over 2004. For all observed lightning discharges in all images, a validating weather radar echo is searched in the corresponding weather radar products. The search radius in units of image pixels (2.4 km) can be changed and the spatial tolerance of the quantitative comparison can thus be adjusted. For each observed lightning discharge the maximum weather radar reflectivity value within the search area is stored. Figure 3.3 shows

histograms of the maximum radar reflectivity for all discharges, i.e., CC and CG discharges, in August 2004. The different curves are obtained for different search radii between 0 and 9 image pixels (22 km). For search radii larger than 2 pixels, the histogram exhibits two distinct peaks: one centered around −1 dBZ and one around 47 dBZ. The lightning discharges contained in the latter peak are clearly associated with strong convective phenomena and are thus most likely true lightning events. The discharges contained in the small peak around −1 dBZ are not validated by a nearby radar reflectivity (−1 dBZ is the lowest reflectivity value in the radar composites) and are probably false events. The events in the histogram of Figure 3.3 can effectively be classified as either false or true using a reflectivity threshold of 7 dBZ. Roughly 1.4% of the detected lightning events in 2004 is classified as false in this way, i.e., a False-Alarm-Ratio (FAR) of 0.014 is found for the SAFIR system.

3.4 Validation against the echotop product

The main disadvantage of using the low-altitude reflectivity composites for validation of the observed lightning discharges is that discharges originating from high altitudes, e.g.

from anvils of thunderstorms, may erroneously be classified as false. Therefore, the echotop height product is most likely (even) better suited for validation of lightning discharges. At KNMI the operational echotop product is determined using a reflectivity threshold of 7 dBZ which fortunately matches the optimum reflectivity threshold for lightning validation. The echotop product provides the "maximum height" as an additional quantity for validation of the observed lightning discharges. Figure 3.4 shows the histograms of the maximum echotop heights for all discharges (CC+CG) in August 2004. Again histograms for different search radii in units of image pixels are shown in the figure. For all search radii (0-9) the histogram clearly exhibits two distinct peaks: one peak centered at 0 km and another peak somewhere between 9 and 12 km. Evidently, the lightning discharges contained in the latter peak are associated with strong convective events for which echotop heights above 10 km are quite common. The peak around 0 km contains events for which no validating radar echo was found and these are thus classified as false events. The clear separation between the two peaks in the histogram, even for zero search radius, suggests that the spatial overlap between the lightning discharges and the echotop patterns is very good. The use of radar data from all heights, and not only from a low altitude, is the rationale for this better spatial overlap. The events in the histogram of Figure 3.4 can effectively be classified as either false or true using an echotop height threshold of 2.0 km. Only 1.0% of the detected lightning events in 2004 is classified as false in

Table 3.2: Results of validation over 2004

Month	Total	False	FAR
January	766	47	0.061
February	1215	8	0.007
March	930	20	0.022
April	36695	130	0.004
May	5007	70	0.014
June	25739	345	0.013
July	125586	980	0.008
August	99615	818	0.008
September	7792	248	0.032
October	6978	305	0.044
November	336	91	0.271
December	292	72	0.247
2004	**310951**	**3134**	**0.010**

this way, i.e., a FAR of 0.010 is obtained for the SAFIR system.

3.5 Discussion

Although a weather radar does not measure the lightning discharges directly, a strong correlation between the radar reflectivity and the presence of lightning discharges is expected and was also observed. The radar reflectivity is a measure for the strength of the convection (updrafts) and the amount of moisture in the atmosphere, and strong updrafts of moist air are the main drive behind lightning activity. Validation of the observed lightning discharges with the most common weather radar product, the low-altitude reflectivity composite, showed promising results. The spatial correlation between the observed discharges and the reflectivity patterns is good. The lightning events can readily be classified as either false or true based on the local maximum reflectivity using a threshold of 7 dBZ.

The main disadvantage of using the low-altitude reflectivity composites for validation of the observed lightning discharges is that discharges originating from high altitudes, e.g. from anvils of thunderstorms, may erroneously be classified as false. The echotop product composed of data from all heights is, therefore, (even) better suited for validating lightning discharges. The echotops should be determined using a reflectivity threshold of 7 dBZ. Indeed, a better separation between the false and true lightning events is seen and a very good spatial overlap between the lightning discharges and the echotop patterns is found. The optimum threshold on the local maximum echotop heights is determined to be 2.0 km

In the Table 3.2 the results of the validation of the SAFIR lightning data against the weather radar echotop product are listed. The total number of observed discharges, the number of false discharges, and the FAR are given. The column with the total number clearly reveals the expected annual evolution of lightning activity. The number of false events is generally rather small both in absolute and relative sense. Only for November and December 2004 an exceptionally large number of false events is found. A further investigation revealed that these false events are probably

Figure 4.1: The KNMI micro-barometer; a differential pressure sensor based on Validyne pressure transducer.

due to a single aircraft with a malfunctioning transmitter.

In conclusion, the weather radar echotop product is especially suited for the validation of the observed lightning discharges. For the SAFIR lightning detection network of KNMI, a FAR of 0.010 is obtained for 2004 in this way. It should be noted, however, that the Probability-Of-Detection (POD) of the lightning detection system, i.e., what is the probability that a real lightning event is actually detected by the system, cannot be assessed using weather radar products for validation.

4. INFRASOUND

Figure 4.2: The field installation of a micro-barometer with noise reducer attached constructed of soaker hose. The micro-barometer is mounted beneath the earth's surface for temperature stability and robustness.

Infrasound is inaudible sound with frequencies below the human hearing threshold of 20 Hz. The lower frequency cut-off of infrasound is limited by the thickness of the atmosphere or a ducting atmospheric layer. In general, infrasound is measured within a frequency range of 0.002 (500 s) to 20 Hz. Within this frequency band many sources of known and unknown origin generate infrasound. Impulsive sources are for example: sonic booms, explosions, nuclear tests, meteors, thunderstorms, and lightning. Sources that can often be detected for hours or days are: volcanoes, sea waves, mountain associated waves and aurora.

In this study we analyze the infrasonic signature of thunderstorms and lightning this will be exemplified by the processing of specific events.

4.1 Infrasound measurement technique

Infrasound can be measured with either a low frequency microphone or a high frequency barometer. KNMI chose to develop a micro-barometer because of its robustness with respect to the field application and durability. Furthermore, a micro-barometer can measure down to much longer periods than a microphone. Figure 4.1 shows the differential micro-barometer: this sensor measures air pressure fluctuations with respect to the pressure in the backing volume. Within the backing volume a capillary is mounted that acts as leak back to the atmosphere. The acoustic resistance of the capillary determines the lowest frequency the micro-barometer can measure, currently 0.002 Hz. The pressure sensitivity is on the order of hundreds of Pa.
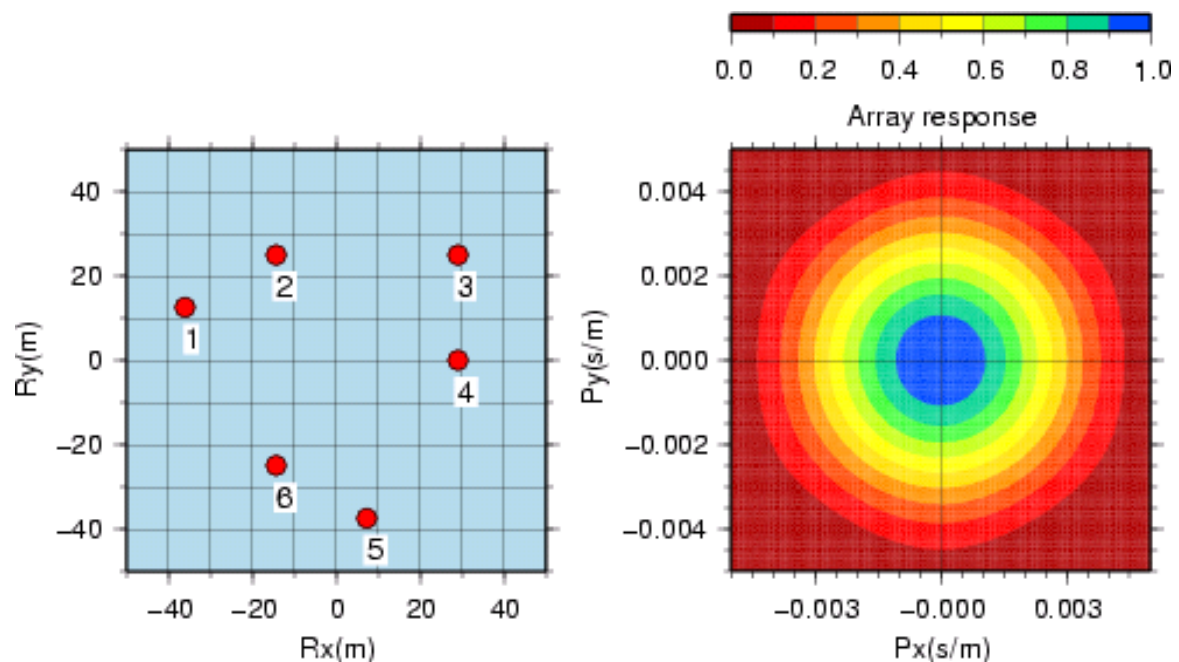
Figure 4.3: Layout of the De Bilt Infrasound Array (DBN) and its response to a 2 Hz plane wave.

Measuring infrasound means dealing with wind noise. Therefore, arrays of micro-barometers are used to increase the Signal-to-Noise Ratio (SNR). Furthermore, arrays enable the determination of source characteristics like: apparent sound velocity and direction of arrival or back azimuth. A source can be localized by triangulation of the observed back azimuths from two or more arrays.

Wind noise is further reduced by applying an analog filter at each array element, i.e. the micro-barometer. Examples of analog filters are large wind screens, soaker hoses, pipe arrays. KNMI applies soaker hose, or porous garden hose, to reduce wind noise at each micro-barometer, see Figure 4.2. By applying this technique, the pressure field is averaged over an area rather than measured at one point. Doing so, incoherent wind noise will cancel while the signal of interest, with much larger coherency lengths, will remain unaffected.

A series of micro-barometers forms an array configured in such a way that an isotropic response is achieved. Figure 4.3 shows the layout and the calculated response to a 2.0 Hz plane wave, of the De Bilt Infrasound Array (DBN). DBN consists of six micro-barometers in a 65 meters aperture layout.

4.2 Thunderstorms and infrasound

A severe thunderstorm passed DBN on 24 August 2004. The raw infrasound recordings are displayed in the left frame of Figure 4.4 containing the full pass-band of 0.002 to 20 Hz. A variety of frequencies of pressure changes occur during the one hour of data displayed in the figure. The longest periods of changes correspond to the instrument response being limited to 500 seconds. Here we will focus on the frequency band of 1 to 20 Hz, where individual events are visible that are associated with the thunderstorm. The data in the right frame of Figure 4.4 are filtered with a second order Butterworth filter with corner frequencies of 1.0 and 20 Hz. The spikes correspond to the electrical discharges on the instruments, an example occurs around 1100 seconds. The transient signal between e.g. 1600 and 1900 seconds corresponds to the thunder and infrasound from lightning discharges.

4.3 Infrasound data processing

Infrasound data are processed by making use of array processing techniques like: signal detection and beam forming (Evers and Haak, 2003). The coherency of the signals is measured to trigger a detection. When all micro-barometers of DBN measure a similar waveform with a certain time delay, the Fisher ratio (Melton and Bailey, 1957), i.e., the square
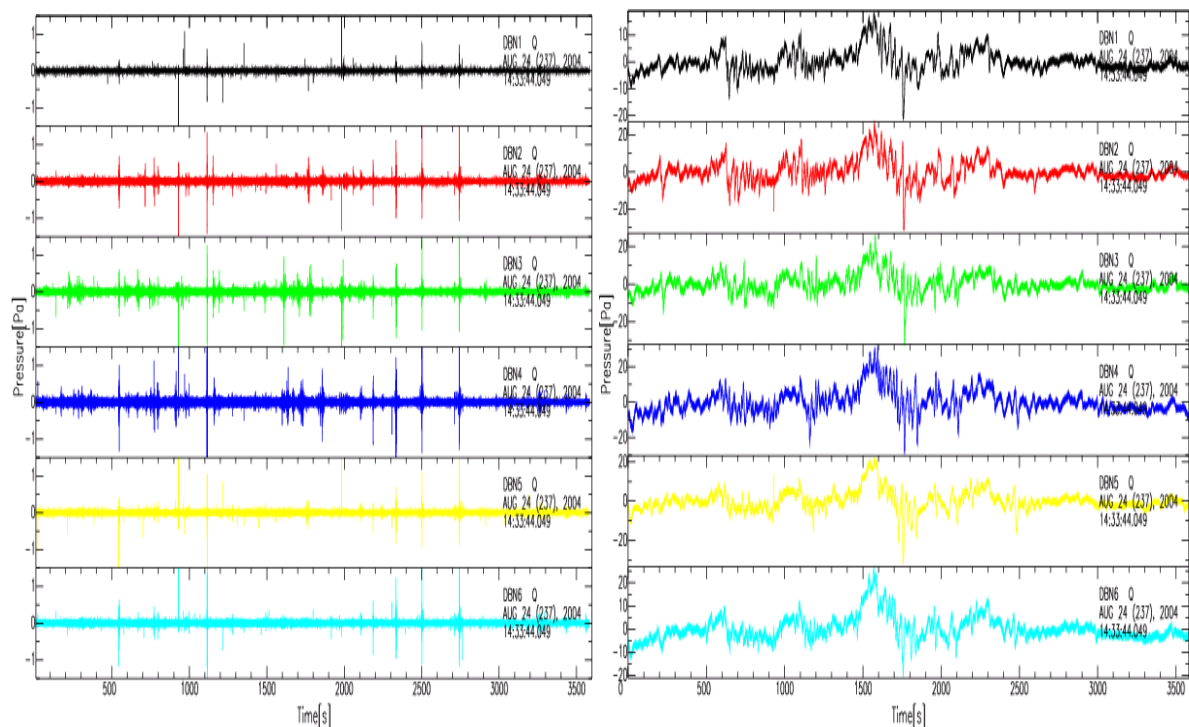
Figure 4.4: Infrasound records of DBN on 2004, July 24, about one hour of data is shown starting at 12:33:44.09 UTC (left frame). Infrasonic data filtered with a second order Butterworth filter having corner frequencies of 1.0 and 20 Hz (right frame).

of the SNR, increases leading to a detection when the absolute value is above some pre-defined threshold value. The time delays are then used to calculate the back azimuth and apparent sound speed of the signals. The apparent sound speed equals the horizontal component of the true sound speed and is a measure of the angle of incidence with respect to the vertical. Therefore, the apparent sound speed can vary between the true sound speed for a horizontally traveling wave and infinity for a vertically traveling wave. The various parameters mentioned are quantified in Figure 4.5 for the segment of data shown in Figure 4.4 (right frame). The lower frame shows the Fisher ratio or SNR power. The red dots correspond to a Fisher ratio higher or equal to 5 and are thus events with a significant coherency. The middle two frames give the resolved apparent velocity and back azimuth (east of north). Again, red dots correspond to events with a significant coherency. The top frame shows one trace of the DBN array.

4.4 Comparison with the SAFIR network

Locations of discharges are measured with the lightning detection network. In Figure 4.6

circles represent these locations with respect to DBN in a polar graph. Small circles are used for Cloud-Cloud (CC) discharges while large circles correspond to a Cloud-Ground (CG) discharge. The colors indicate the time of occurrence with respect to 12:33:44.09 UTC, the starting time as used for the infrasound analysis. Overlaid are the observed infrasonic back azimuths in DBN, the colored bearing. The early developments within the thunderstorm appear to the northwest of DBN where also corresponding back azimuths are found (i.e. blue colors). With ongoing time activity turns to the south, the infrasound observations follow these later developments (i.e. red colors).

4.5 Discussion

The first results on the comparison of measurements of the lightning detection network and infrasound observation show promising results. Infrasound from discharges and thunder can be associated over a distance of at least 40 km.

Further research will focus on:
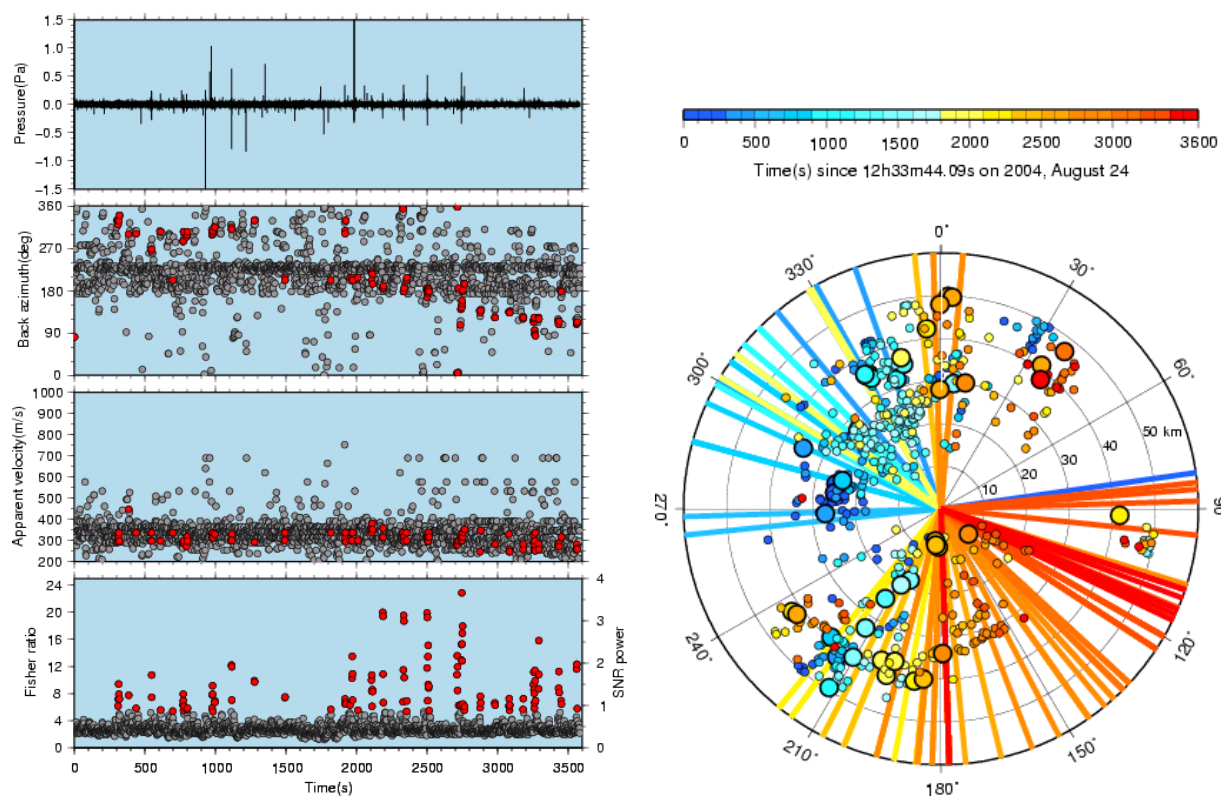• Identification of what part of the infrasound

Figure 4.5 (left): Typical analysis of infrasound data. The red dots correspond to a Fisher ratio higher or equal to 5 and are events with a significant coherency.

Figure 4.6 (right): Rose diagram showing direction as a function of distance with respect to DBN. The circles give the observations from the lightning detection network as function of time (color coded), small circles for cloud-cloud discharges and large ones for surface-cloud discharges. The bearings represent the observed back azimuths from DBN.

is associated with the detection by the lightning network

- Use of the travel times of the infrasonic signals to confirm the source location.
- Investigation of the infrasonic waveforms in detail to discriminate between CC and CG discharges and thunder.

5. LOFAR

LOFAR, the Low Frequency Array (www.lofar.org), is a next-generation radio telescope in The Netherlands. It will initially operate at frequencies from 30 to 240 MHz (corresponding to wavelengths of 10 to 1.2 m). Its superb sensitivity, high angular resolution, large field of view, and flexible spectroscopic capabilities will be a dramatic improvement over previous telescopes at these wavelengths. As such, the LOFAR telescope will enable a broad range of fundamental astrophysical studies.

The design, development, and construction of the telescope are being driven by four key astronomical projects designed to pursue LOFAR science of fundamental importance:

- The Epoch of Re-ionisation
- Extragalactic Surveys and their exploitation to study the formation and evolution of clusters, galaxies and black holes
- Transient Sources and their association with high energy objects such as gamma ray bursts
- Cosmic Ray showers and their exploitation to study the origin of ultra-high energy cosmic rays
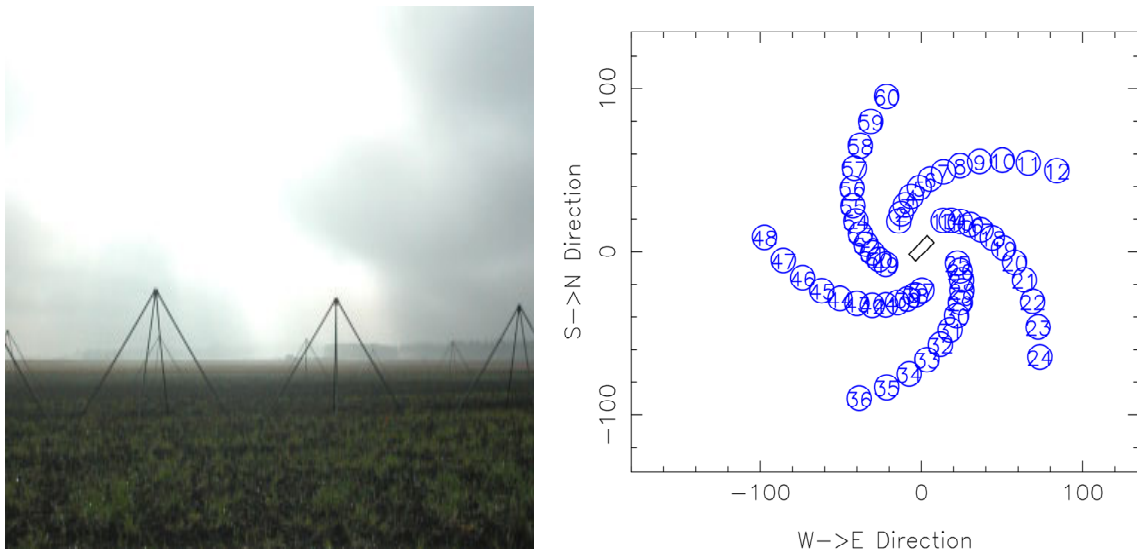
Figure 5.1: Photo of LOFAR antennas at the Initial Test-Station (ITS) and the antenna layout of the LOFAR Initial Test-Station (right). The individual antennas are arranged in a log-spiral pattern.

In December 2003 the Initial Test Station (ITS) for LOFAR became operational as an engineering array. It is located near the village of Exloo at the site of the future compact core of the LOFAR telescope. Since its commissioning ITS has been used for a variety of experiments both scientific and educational in nature (Wijnholds 2005). In April 2005 the core of the LOFAR Central Processor (CEP), an IBM BlueGene/L system the fastest supercomputer in Europe at time of installation, was officially taken into operation at the Compute Centre of the Rijksuniversiteit Groningen.

The construction of the LOFAR telescope is scheduled to start at the beginning of 2007, with the compact core being fully operational by 2008. After that the remote stations will be added to the array, summing up to a total of 77 stations with 96 dipoles each. Finally, the extension of LOFAR to other European countries will increase the baselines to some 1000 km and hence improve the resolution by another order of magnitude.

5.1 Experimental setup

LOFAR-ITS consists of 60 signal paths which can be configured as 60 single dipoles or as 30 crossed dipoles for dual polarization measurements. The ITS antenna layout is shown in Figure 5.1. The incoming radio signals are filtered by a 10 – 35 MHz band-

pass filter, digitized at a sample rate of 80 MHz, and passed on to a 512 mega-sample cyclic RAM buffer. The contents of this buffer can be saved to disk and the moment of data capture can be set by an external trigger.

While for the fully operational LOFAR telescope streaming data will be processed at both station and central processor level, LOFAR-ITS only allows processing of consecutive snapshots of the cyclic RAM buffer. The duty cycle is limited by the writing speed of the hard-disks. The data files, a 6.7 seconds snapshot amounts up to 60 Gb, are transferred to ASTRON for further processing.

When a (severe) thunderstorm in the northern Netherlands was apparent on the weather radar imagery, a random series of data capture triggers was submitted to the data acquisition system of LOFAR-ITS. In this way, a considerable number of lightning discharges could be recorded with the prototype LOFAR station.

5.2 Data processing

Data analysis and processing is performed using the LOPES-Tools, a software package initially developed and written for the LOPES experiment (Falcke *et al*, 2005). The standard procedure for each recorded data set is:

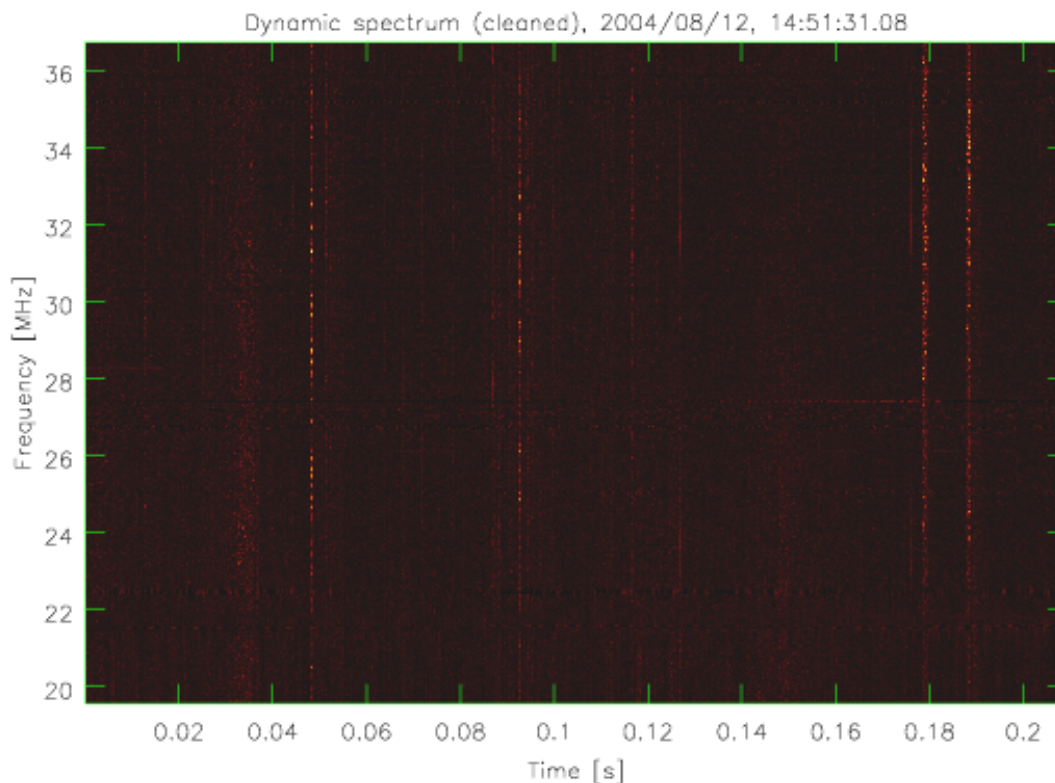1. Inspection of the raw digitized time series to identify "bad" antennas, i.e., antennas

Dynamic spectrum (cleaned), 2004/08/12, 14:51:31.08

Figure 5.2: Dynamic spectrum I(t, ν) of total power for one of the data sets recorded on 12 August 2004. The time resolution is 0.2048 ms and the frequency resolution is 0.0488 MHz. The lightning events (pulsed broad-band emission) appear as vertical lines in this spectrum.
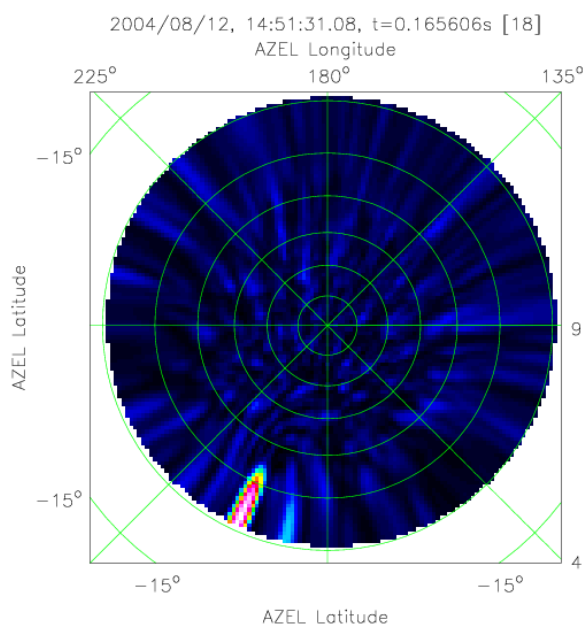
2004/08/12, 14:51:31.08, t=0.165606s [18]

Figure 5.3: All-sky map showing the source for the brightest peak in the dynamic spectrum shown in Figure 5.2.

with a received power deviating more than three standard deviations from the mean. These antennas are flagged and excluded from subsequent processing.

2. Generation of a dynamic spectrum. This is done by splitting the data into chunks of $N_{Blocksize}$ samples and stacking the summed power spectra:

$$I(t,v) \equiv I[k_m] = \frac{1}{N_{Ant}} \sum_j \overline{\tilde{f}_j[k_m]} \cdot \tilde{f}_j[k_m]$$

where $f_j[k_m]$ is the Fourier transform of the m-th data block of antenna j. The resulting dynamic spectrum allows assessment of the overall radio frequency environment.

3. Division of the dynamic spectrum by the time-averaged spectrum provides a simple way to reject Radio Frequency Interference (RFI). An example of an RFI-cleaned spectrum is shown in Figure 5.2. The lightning events (pulsed broad-band emission) appear as vertical lines in this spectrum.
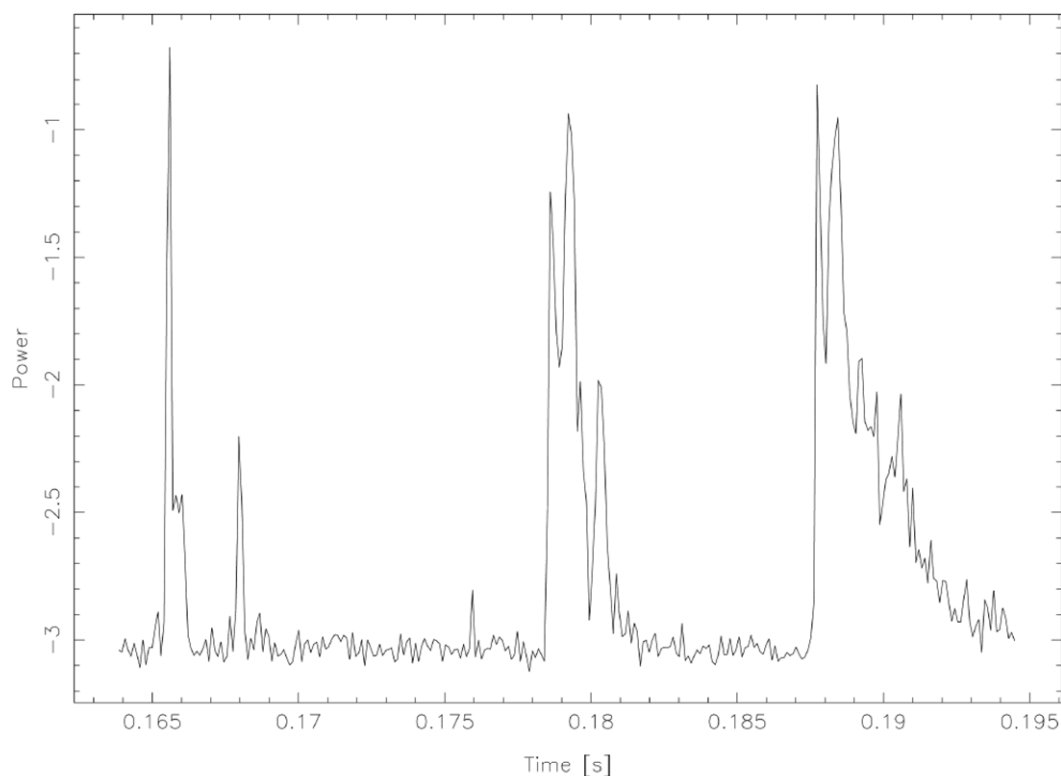
Figure 5.4: Total power as function of time for a beam towards the position of a lightning discharge.

4. Generation of an all-sky map showing the direction of the lightning discharge (see Figure 5.3). Subsequently, a high-resolution map centered on the identified discharge providing the intensity as function of azimuth, elevation, distance, and time can be calculated. This map enables study of the spatial-temporal fine structure of a discharge (see Figure 5.4).

In the future the procedure described above will be implemented as an automated pipeline delivering the following products:
1. Dynamic spectrum (raw and RFI cleaned)
2. Time series of total power
3. Multi-dimensional all-sky maps with azimuth, elevation, distance, and time
4. Source location (azimuth, elevation, distance)
5. Pulse profile of the lightning discharge.

5.3 Comparison with SAFIR data

A first comparison of the LOFAR-ITS observations and those from the SAFIR lightning detection network of KNMI has been made. For this purpose, data recorded during a severe thunderstorm on 12 August 2004 have been used. Due to the prototype nature of LOFAR-ITS, only 2 seconds of data in a 20 minute period could be recorded. The cleaned dynamic spectra show a large number of pulsed broad-band features, as typically expected from a lightning discharge (see Figure 5.2), and which were not seen under clear weather conditions. About 22 lightning

Table 5.1: Number of (matching) events from LOFAR-ITS and SAFIR for 12 August 2004. The total time coverage of the ITS snapshots is 2.1 seconds.

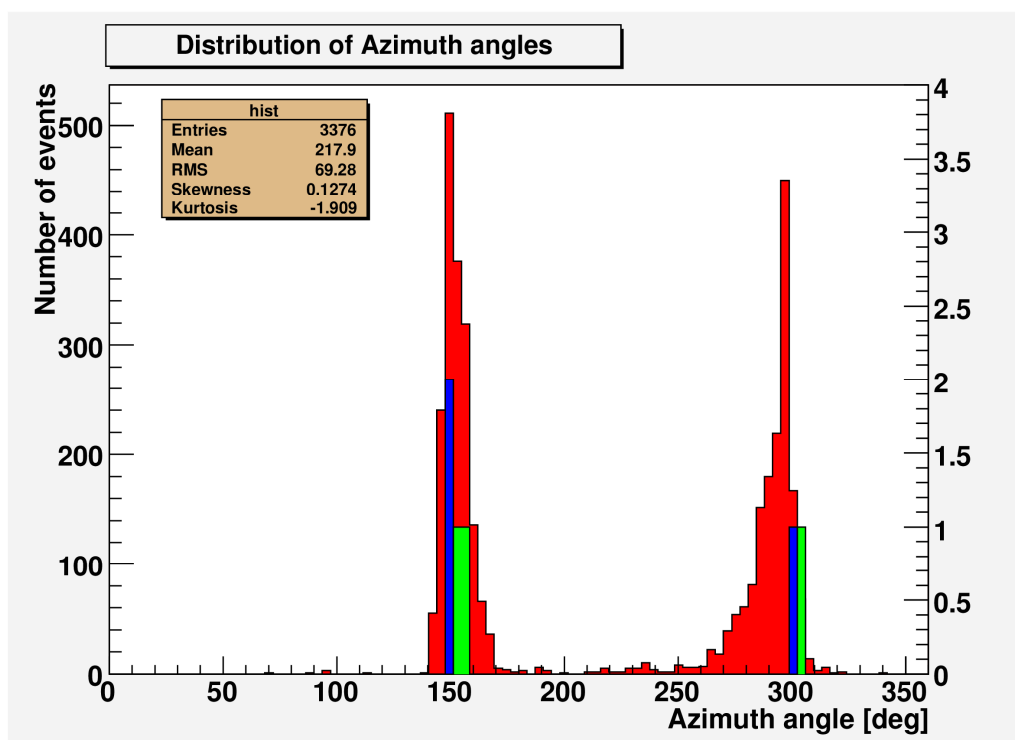| Time [UTC]	ITS	SAFIR
14:51:31.08	3 (0)	0 (0)
14:53:59.92	2 (1)	1 (1)
14:58:25.92	4 (0)	0 (0)
15:02:51.82	3 (2)	2 (2)
15:06:26.94	6 (1)	1 (1)
15:10:05.50	4 (0)	0 (0)
Total	**22 (4)**	**4 (4)**

Figure 5.5: Histogram of lightning events as function of azimuth between 14:45 and 15:15 UTC on 12 August 2004. All events detected by SAFIR are displayed in red, and the matched events are shown in blue and green for the azimuths from SAFIR and LOFAR-ITS, respectively.

events with a good signal-to-noise ratio were detected within the 2 second time frame.

The lightning discharges recorded by LOFAR-ITS have been compared with the data from the SAFIR lightning detection system. The results of this comparison are summarized in Table 5.1. The table lists the number of events in each snapshot and the number of matching events between the brackets. Out of the 22 events, three lightning events could be matched by their time stamps and direction (see Figure 5.5). One additional event could be identified by a simple comparison of the time stamps. It is evident from the table that the number of events observed by LOFAR-ITS is much larger than the number of discharges localized by SAFIR during this period. Moreover, all lightning discharges observed by SAFIR are validated by the LOFAR-ITS data. The triangulation performed by the SAFIR system will cause a rejection of (weak) discharges which cannot be localized. The lower number of SAFIR events is, therefore, probably caused by this triangulation and a lower sensitivity of the antennas. Of course,

the events observed by LOFAR-ITS need further investigation and validation.

5.4 Discussion

LOFAR is expected to provide a considerable contribution to the monitoring and study of radio emission from lightning discharges. Due to the significant increase:
➢ in density of geographic coverage with respect to the SAFIR lightning detection network, and
➢ in the number of reception elements (77 times 96 antennas instead of 4 times 5 antennas for SAFIR)
a far larger number of (weaker) discharges can be detected. The longer baselines and higher signal sampling frequency will enable a more precise reconstruction of the spatial-temporal evolution of radio-emissive processes in a thunderstorm. Since LOFAR maintains phase-coherence between its stations the obtainable spatial resolution for lightning detection should also increase linearly with station separation and might improve from degrees to fractions of arcminutes. For the lightning events discussed here this could lead

to a localization accuracy of approximately 50 meters with a very high time resolution.

6. REFERENCES

Beekhuis, H., and I. Holleman, 2004: Upgrade and evaluation of a lightning detection system. International Lightning Detection Conference 2004, Vaisala.

Doviak, R.J., and D.S. Zrnić, 1993: Doppler Radar and Weather Observations. 2nd edition, Academic Press, San Diego.

Evers, L.G., and H.W. Haak, 2003: Tracing a meteoric trajectory with infrasound. *Geophys. Res. Lett.*, **30**, ASC 1-4.

Falcke, H., *et al*, 2005: Detection and imaging of atmospheric radio flashes from cosmic ray air showers. *Nature*, **435,** 313-316.

Holleman, I., 2001: Hail detection using single-polarization radar. KNMI Scientific Report WR-2001-01.

Holleman, I. 2005: Quality Control and Verification of Weather Radar Wind Profiles. *J. Atmos. Ocean. Technol.,* **22**, 1541-1550.

Melton, B.S., and L.F. Bailey, 1971: Multiple signal correlators. *Geophysics*, **XXII**, 565-269.

Roozekrans, H., and I. Holleman, 2003: KNMI HDF5 Data Format Specification v3.5. KNMI Internal Report IR-2003-05.

Wijnholds, S., 2005: One year in the bushes: Results from ITS. Technical Report LOFAR-ASTRON-RPT-052, ASTRON.

7. CONCLUSIONS

In this paper the preliminary results of the validation of lightning data from the KNMI-SAFIR system of with weather radar products, data from infrasound arrays, and retrievals from the LOFAR Initial Test-Station (ITS) have been presented. The weather radar echotop product is especially suited for the validation of the observed lightning discharges. For the SAFIR lightning detection network of KNMI, a False-Alarm-Ratio (FAR) of 0.010 is obtained for 2004. The Probability-Of-Detection (POD) of the lightning detection system cannot be determined using weather radar data. The first comparison of infrasound observations of thunder with data from the lightning detection network shows promising results. Infrasound from thunders and discharges from lightning can be associated over a distance of at least 40 km. The LOFAR telescope array with its very long baselines and its high signal sampling frequency will enable a precise reconstruction of the spatial-temporal evolution of the radio-emissive processes in a thunderstorm.

All in all, it is concluded that these three remote sensing systems provide a wealth of information on different aspects of lightning and thunder. This information may help to improve the performance of lightning detection systems and to increase our understanding of the complex processes inside a thunderstorm.